## PAPER

Check for updates

# CL-20/TNT decomposition under shock: cocrystalline *versus* amorphous

Yan Li, [ID] *[ab] Wen-Li Yu[a] and Huang Huang[b]

The cocrystallization strategy is considered to be an effective means to adjust the properties of explosives. Nevertheless, the underlying mechanism of the effect of the special cocrystal structure on the decomposition process is not clear enough. The present work compares the response processes of a CL-20/TNT cocrystal structure and an amorphous structure under shock waves with different velocities. The thermodynamic evolution, reactant decay, product formation, main initial reactions and cluster evolution are analyzed. As a result, we find that the amorphous structure is easier to compress than the cocrystal structure, achieving higher stress and temperature. These thermodynamic parameters have a strong correlation. For the amorphous structure, the chemical reaction of the system is more intense, the reactants decay faster, the products are more abundant, and the intermediate products can complete the transformation to stable products earlier. Furthermore, $NO_2$ is the most important intermediate product, and its quantitative change can directly reflect the reaction process. The amorphous structure is more prone to decomposition reaction, and the cocrystal structure is more prone to polymerization reaction. The cluster size in the amorphous structure is smaller and more conducive to decomposition.

## 1 Introduction

Explosives play an important role in both military and civil fields. People's demand for explosives has changed from blindly pursuing great power to considering power and security. This requires that energetic materials not only have high energy density but also have low sensitivity. However, there is an obvious power-safety contradiction for explosives. To solve this contradiction, scientists have carried out a lot of work, among which the cocrystallization strategy has attracted extensive attention. Recently, Zhang systematically explained the definition of a cocrystal. A cocrystal refers to a single phase crystalline solid composed of two or multiple components in a stoichiometric ratio, and the components of a cocrystal can be atoms, molecules, anions and cations in pairs, and/or metallic cations with free electrons shared.[1] The cocrystallization strategy can change the assembly and arrangement of molecules and reconcile energy density and sensitivity.[2]

CL-20 has the highest energy density among the explosives that can be mass produced at present, but its high sensitivity greatly limits the wide application. Many studies focus on the desensitization of CL-20, and cocrystallization strategy just meets this demand. In 2011, Bolton and Matzger prepared CL-20/TNT energetic cocrystal, a milestone work.[3] The material has the respective characteristics of CL-20 and TNT. It not only maintains a good energy density but also has a significantly reduced sensitivity compared with CL-20. After that, a variety of cocrystals based on CL-20 were prepared.[4–15] Their preparation expanded a new direction for the development of CL-20 and brought CL-20 closer to large-scale use.

In addition to preparation, people are curious about the reasons why cocrystal explosives can show excellent comprehensive properties. Shreeve pointed out there are still some fundamental issues associated with structure–property relationships of energetic cocrystals that needed to be explored.[16] To explore the internal mechanism of cocrystallization strategy for the improvement of explosive properties, scholars have carried out a lot of research by using theoretical analysis, simulation calculation and other methods. Zhang and his team systematically explained the mechanism of cocrystallization strategy on the performance reconciliation of explosives. Firstly, they analyzed the energy and safety characteristics of a variety of energetic cocrystals. The results show that the power is diluted but the safety may be improved after cocrystallization in contrast to the more energetic pure component.[17] For the study of the structure, electronic and energy features of CL-20 based cocrystals, they found that relative to the pure CL-20 polymorphs, the cocrystallization of CL-20 with HMX, TNT and BTF cause little molecular deformation except some torsion of its nitro groups, and the narrower band gaps.[18] Subsequently, the team carried out a lot of research on the intermolecular interactions of cocrystals.[19–23] These studies have a deeper understanding of cocrystals from the perspective of crystal

*[a]Xi'an High-Tech Research Institute, Xi'an, 710025, China*

*[b]Naval University of Engineering, Wuhan, 430033, China*

engineering and provide theoretical support for the design and composition selection of cocrystals.

In the process of actual production, storage, transportation and use, explosives are often likely to suffer from external stimuli. Especially heat and shock, under the action of these two common stimuli, the response of cocrystal explosives is of concern. Guo compared the thermal decomposition of the TNT/CL-20 cocrystal with pure crystals of TNT and CL-20 and with a simple physical mixture of TNT and CL-20.[24] This research found that cocrystallization well reconciled the performance of the two components, which is difficult to achieve in a physical mixture system. Xue compared the thermal decomposition of the CL-20/HMX cocrystal with the pure crystals of CL-20 and HMX.[25] It is found that the initial decay steps in pure crystals remain still in the cocrystal. The heat transfer caused by different decay rates between components is the essence of cocrystallization's mediation. Through the analysis of thermal decomposition of two typical cocrystals processes of CL-20/TNT and CL-20/HMX, Ren summarized three stages of CL-20 based cocrystals thermal decomposition: the first stage is the fracture of N–NO$_2$ bonds and the destruction of cage skeletons, the second stage is the secondary reaction of the initial products, and the third stage is the rapid consumption of intermediate products to form stable products.[26,27] Liu studied the initial decomposition mechanism of CL-20/HMX cocrystal under steady shock wave.[28] The results show that after the application of the shock wave, the cocrystals successively undergo an induction period, fast compression, slow compression, and expansion processes. Zhang performed quantum based multi-scale shock simulation under shock loading by self-consistent charge density-functional tight binding method to study the initial chemical mechanism of CL-20/TNT under shock loading.[29] The results demonstrate that the temperature and pressure increase with the decrease of volume when shock strength constantly increases. They also found that NO$_2$ is the dominant primary intermediate resulting from a weak bond barrier. Our previous work focused on the anisotropy of the response of CL-20/TNT cocrystal under shock.[30] The results show that the special layered structure of cocrystal makes the response have clear anisotropy under shock wave.

The existing theoretical researches make people have a certain understanding of the response process of cocrystal explosives under heat and shock. Recently, Sinditskii's experimental study on the thermal decomposition processes of CL-20 based cocrystals shows that the lattice decomposition is an important reason to accelerate the thermal decomposition of CL-20. In the process of thermal decomposition, CL-20 will change into the amorphous structure, which greatly affects its thermal stability.[31] Michael Sakano also conducted a comparative study on the thermal decomposition processes of amorphous and crystalline RDX.[32] The results show that after heating, the crystal undergoes a rapid endothermic process, which is related to the loss of crystal order. The process takes place before chemical decomposition and reduces the actual temperature of the reaction. This makes us very interested in the decomposition process of amorphous structure and cocrystal structure. In this paper, the response processes of CL-20/

TNT cocrystal structure and amorphous structure composed of these two conformers under shock are investigated. A CL-20/TNT supercell model and an amorphous structure model are constructed with the same number of molecules. Using ReaxFF reactive force field molecular dynamics in conjunction with a multiscale shock technology, 6–9 km s$^{-1}$ shock waves are loaded on the two models respectively. The temperature, stress, volume, reactants decay, products formation, initial decomposition paths, and the clusters in the reaction process are analyzed.

## 2 Methods and computational details

The CL-20/TNT co-crystals cell data used in this paper was derived from the X-ray crystal structure.[3] The initial single crystal cell contains 8 CL-20 molecules and 8 TNT molecules. Based on this, the single crystal cell was expanded to a $4 \times 2 \times 1$ supercell, which contains 64 CL-20 molecules and 64 TNT molecules, totaling 3648 atoms.

Firstly, the conjugate gradient algorithm was used to relax the cocrystal structure. The convergence tolerance of force was $10^{-7}$ (kcal mol$^{-1}$) Å$^{-1}$. Subsequently, we carried out a canonical ensemble (NVT) MD simulation for 10 ps at 298 K using Berendsen thermostat to relax the supercell. To obtain the structure at atmospheric pressure, the NPT ensemble is used for 15 ps relaxation at 298 K and 0 GPa, the Nosé–Hoover method is selected for temperature and pressure control. The cocrystal structure of CL-20/TNT at room temperature and pressure is obtained (Fig. 1), the density is 1.89 g cm$^{-3}$.

The amorphous structure is obtained *via* the melt and quench method. We use the non-reactive potential by Smith and Bharadwaj[33] starting from the $4 \times 2 \times 1$ cocrystal supercell. The crystal is heated at 800 K and 0 GPa for 300 ps under the NPT ensemble to ensure that the crystalline order of the cocrystal is completely broken. Then we quenched the structure at 300 K and 0 GPa for 50 ps under the NPT ensemble. After that, the amorphous structure is relaxed using the ReaxFF force field *via* energy minimization. To match the density of cocrystal, the structure is deformed at 300 K under the NVT ensemble. Finally, another NVT MD is conducted at 300 K for 20 ps to relax the sample. We obtain the amorphous structure shown in Fig. 1.

After obtaining the required models, steady shock waves of 6–9 km s$^{-1}$ are applied along $X$ using multiscale shock technology.[34] A total of 8 processes (list in Table 1) are simulated,
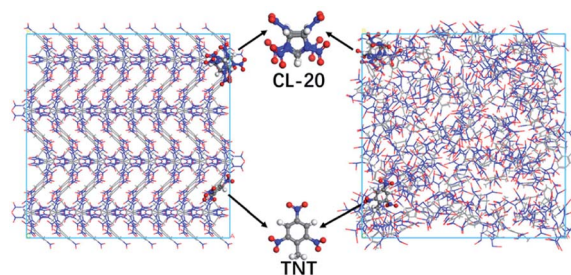


Fig. 1 Cocrystal structure and amorphous structure.

**Table 1** Processes of Simulations

| No | Model | Velocity of shock wave |
|----|-------|------------------------|
| 1 | Cocrystal structure | 6 km s$^{-1}$ |
| 2 | Cocrystal structure | 7 km s$^{-1}$ |
| 3 | Cocrystal structure | 8 km s$^{-1}$ |
| 4 | Cocrystal structure | 9 km s$^{-1}$ |
| 5 | Amorphous structure | 6 km s$^{-1}$ |
| 6 | Amorphous structure | 7 km s$^{-1}$ |
| 7 | Amorphous structure | 8 km s$^{-1}$ |
| 8 | Amorphous structure | 9 km s$^{-1}$ |

and the simulation time is 50 ps. All shock process simulations use the Lammps package, the potential function is ReaxFF/lg,[35] the time step is set to 0.1 fs, and the periodic boundary condition is adopted.

## 3 Results and discussion

### 3.1 Evolution of temperature, stress and volume

The temperature evolutions are shown in Fig. 2. The temperatures rise under various conditions. When the shock wave intensity is low (6 km s$^{-1}$, 7 km s$^{-1}$), the system temperature rises sharply at the beginning and tends to be stable when it reaches a certain value. In this case, under the action of shock wave, the systems have obvious physical changes at the beginning, resulting in the sharp rise of temperature. After that, there is no large-scale chemical reaction and the temperature stabilizes. The temperature rise of amorphous structure is slightly higher than that of cocrystal structure, indicating that the physical changes inside the amorphous structure are more violent. When the shock wave velocity reaches 8 km s$^{-1}$, the temperature of the system rises sharply at the initial stage and then gently rises. In this case, the physical change of the system makes the temperature rise sharply. Then, chemical reaction occurs. The heat released by the chemical reaction makes the system temperature rise at a low rate. It can be found that the temperature rise of amorphous structure is significantly higher than that of cocrystal structure, indicating that the chemical

reaction in amorphous structure system is more intense than that in cocrystal structure system. When the shock wave velocity reaches 9 km s$^{-1}$, the temperature change process of the system goes through three stages, rising sharply in the initial stage, then rising at a high rate, and finally rising at a low rate. In this case, after the physical change, a large-scale chemical reaction occurs, releasing a large amount of heat, and the system temperature rises at a high rate. Finally, as the chemical reaction gradually slows down, the temperature rise rate also decreases. Moreover, in the second large-scale chemical reaction stage, for amorphous structure, in addition to higher system temperature, the time required to enter the third stage is also shorter, which indicates that the chemical reaction of amorphous structure is stronger and can complete the large-scale reaction in a shorter time.

The stress evolution under shock wave loading is shown in Fig. 3. When the shock wave intensity is not high (6 km s$^{-1}$, 7 km s$^{-1}$, 8 km s$^{-1}$), the stress of the system first increases to a certain value and then tends to be stable. The stronger the shock wave is, the higher the stress value in the stable state is. At the same time, the stable stress of amorphous structure is slightly higher than that of cocrystal structure. When the shock wave velocity reaches 9 km s$^{-1}$, the stress of the system reaches a certain value at the beginning, then increases gently, and finally decreases gradually.

The volume evolution under shock wave loading is shown in Fig. 4. The volume is the ratio of the current volume to the volume before compression, which is the degree of compression of the system. When the shock wave intensity is not high enough (6 km s$^{-1}$, 7 km s$^{-1}$, 8 km s$^{-1}$), the system volume tends to be stable after being compressed to a certain extent. The degree of compression of amorphous structure under the action of shock wave with the same strength is significantly higher than that of cocrystal structure. For the cocrystal structure, the maximum compression ratios are 0.78, 0.73, and 0.69 when shocked with the velocities of 6, 7, and 8 km s$^{-1}$ during the first 50 ps. For the amorphous structure, the maximum compression ratios are 0.74, 0.70, and 0.64 when shocked with the velocities of 6, 7, and 8 km s$^{-1}$ during the first 50 ps. When the shock wave
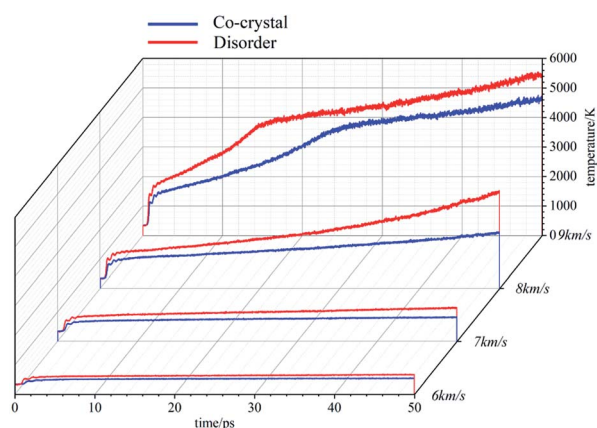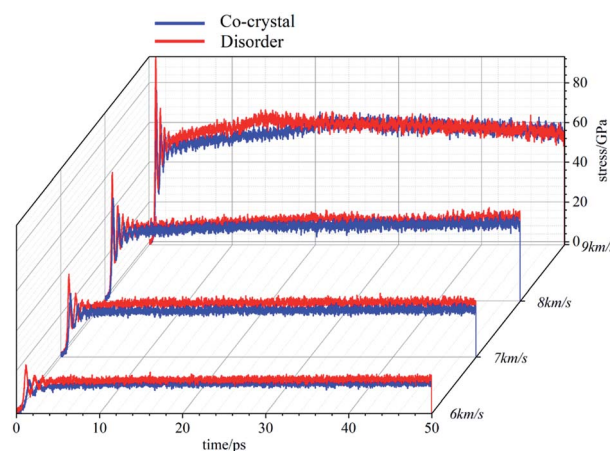


**Fig. 2** Evolution of temperature.
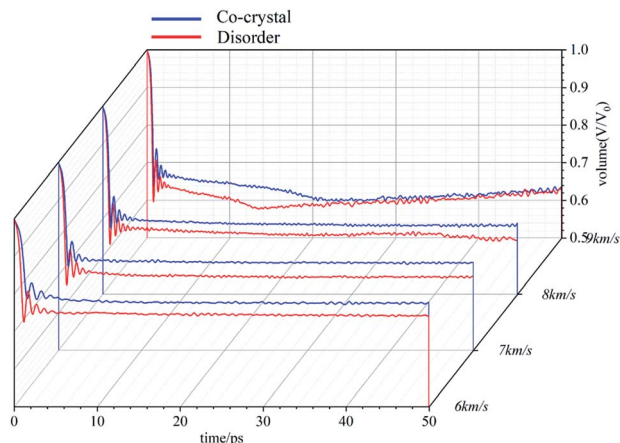


**Fig. 3** Evolution of stress.
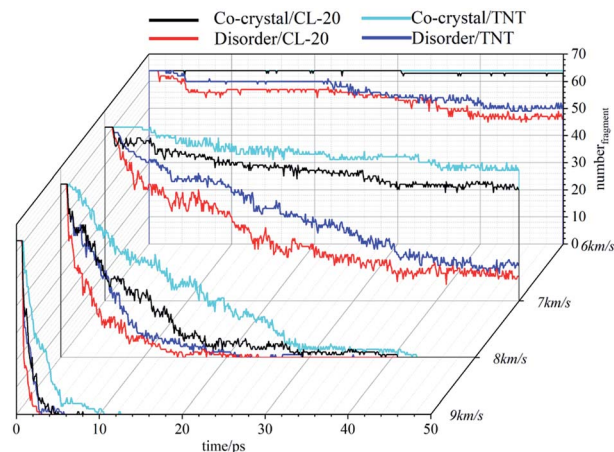
Fig. 4 Evolution of volume.



Fig. 5 Evolution of reactants.

velocity reaches 9 km s$^{-1}$, the volume change of the system also goes through three stages: sharp compression in the first stage, continuous compression in the second stage and slow expansion in the third stage.

Under the action of shock wave, cocrystal explosives will be compressed to produce stress. Under the stress, the system will change physically, resulting in the rise of temperature. The higher compressibility lead to higher stress and higher temperature. When the temperature reaches a certain degree, chemical reactions occur in the system. The heat released by the chemical reaction will further increase the temperature, which corresponds to the increase of compression and stress. Therefore, the changes of temperature, stress and compression degree of the system have strong linkage. For the same system, the times corresponding to the inflection point of the three evolution curves coincide. Amorphous structure is easier to compress than cocrystal structure, resulting in greater stress, higher temperature and more violent chemical reaction (if any). Each stage of the evolution process also comes earlier than cocrystal structure. This indicates that the reaction energy barrier is lower in the amorphous structure than the cocrystal structure which is consistent with the experimental results.[31]

## 3.2 Reactants and products

**3.2.1 Reactants.** Fig. 5 shows the decay of reactants CL-20 and TNT with time in cocrystal system and amorphous structure system respectively. When the shock wave velocity is 6 km s$^{-1}$, CL-20 and TNT in the cocrystal structure are almost not consumed, while the two reactants in the amorphous structure are consumed to a certain extent (within 50 ps, CL-20 is consumed by 25% and TNT is consumed by 18.8%). When the shock wave velocity reaches 7 km s$^{-1}$, the reactants of cocrystal structure begin to decay, while the reactants of amorphous structure decay more rapidly. The reaction degree is still not high enough, and all reactants are not completely decomposed within 50 ps. When the shock wave velocity reaches 8 km s$^{-1}$, the reactants can be completely decomposed within 50 ps, and the number of reactants in the amorphous structure can reach 0 in a shorter time. At 9 km s$^{-1}$, the decomposition rate of reactants is faster and almost exhausted within 10 ps. On the whole, for the same reactant, the amorphous structure decomposes more rapidly and thoroughly than the cocrystal structure. In the same system, the decomposition rate of CL-20 was significantly faster than that of TNT.

**3.2.2 Products.** Fig. 6 shows the changes of main products in cocrystal structure and amorphous structure with time. There are few products of cocrystal structure under the shock wave with a velocity of 6 km s$^{-1}$, which is not shown in the figure. It can be observed that under the shock wave with a velocity of 6 km s$^{-1}$, a certain number of $C_{12}H_{12}O_{24}N_{24}$ and $C_{13}H_{11}O_{18}N_{15}$ are produced in the amorphous structure. These two products are combined by two CL-20 molecules, one CL-20 and one TNT molecule respectively. Only a small amount of $NO_2$ and $NO_3$ are produced in the system. At this time, the consumed CL-20 and TNT are mainly combined into larger clusters. At 7 km s$^{-1}$, the amorphous structure decomposes and produces a certain amount of NO, $NO_2$ and $NO_3$, that is, the N–$NO_2$ bonds in CL-20 and the C–$NO_2$ bonds in TNT break. A certain amount of stable product $N_2$ is also produced in the system. At the same time, the cocrystal structure is still dominated by the combination of reactants, the amount of NO, $NO_2$ and $NO_3$ produced is small. There is no considerable decomposition. At 8 km s$^{-1}$, the amorphous structure undergoes a large-scale decomposition reaction, producing a large number of intermediate products such as NO, $NO_2$ and $NO_3$, which are converted into a large amount of stable product $N_2$. Besides, there are a certain amount of stable products $H_2O$ and $CO_2$ in the system. The emergence of $CO_2$ marks the rupture of the carbon rings of CL-20 and TNT. The system decomposition has reached a high degree. However, $N_2$ in cocrystal structure is relatively small, and $CO_2$ does not appear in the system. At 9 km s$^{-1}$, a certain number of N-containing intermediates NO, $NO_2$ and $NO_3$ are produced both in the two systems at the beginning. Then, the N-containing intermediates gradually convert to stable product $N_2$, resulting in its number gradually decreases. When the number of N-containing intermediates decreases to 0, the number of $N_2$ does not increase significantly. Interestingly, the time point at which $NO_2$ disappears coincides with the time
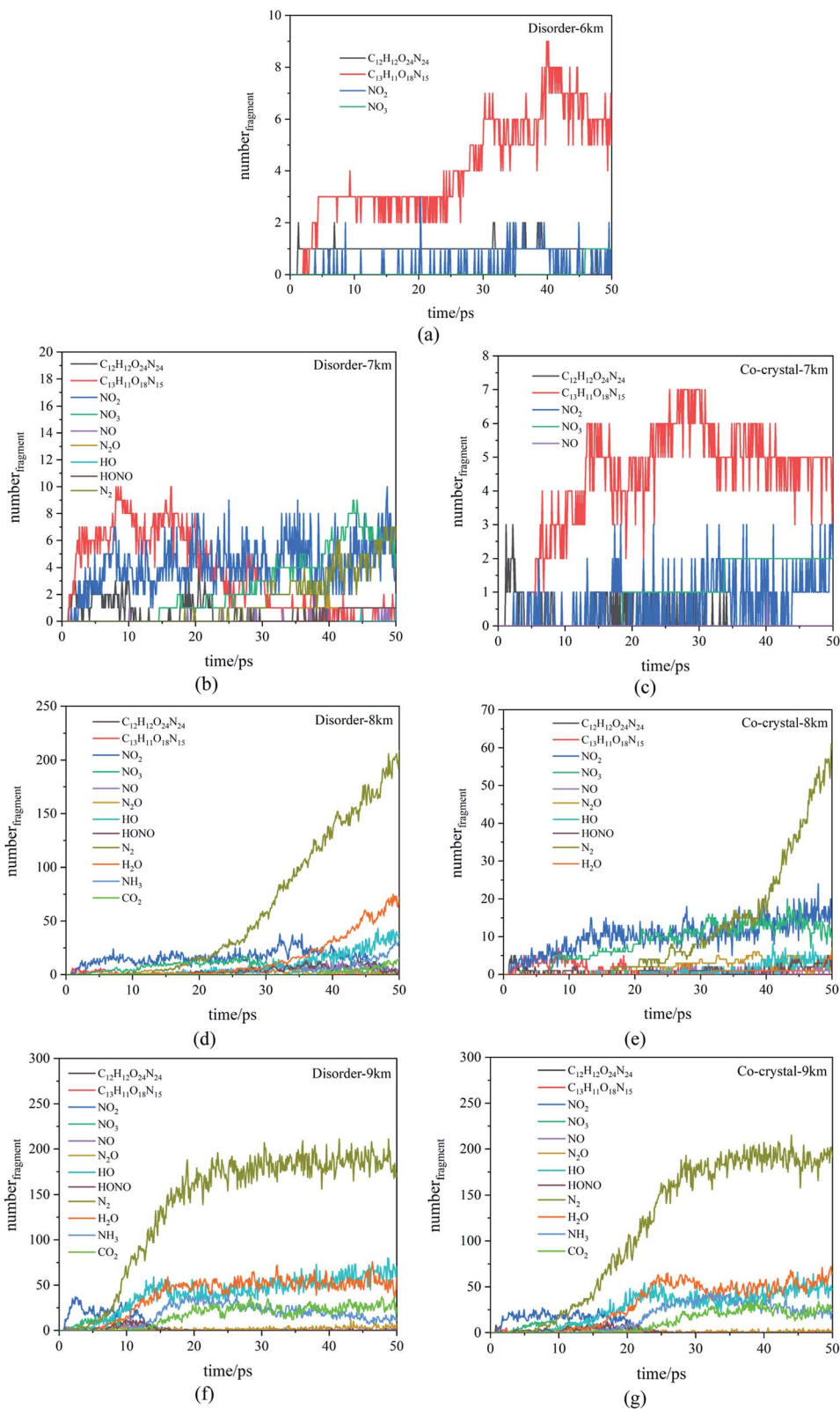
Fig. 6  Evolution of products.

point at which the system volume begins to expand. This shows that the reaction process of the system is highly related to its thermodynamic evolution. $NO_2$ plays an important role in the decomposition, and its quantity can directly reflect the reaction process. In addition, there are a considerable number of stable products such as $H_2O$, $CO_2$ and $NH_3$ in the system. The number

of products in amorphous structure is close to that in cocrystal structure at 50 ps, but the number of products in amorphous structure stabilizes earlier. On the whole, comparing the product evolution of amorphous structure and cocrystal structure, it can be found that amorphous structure is more prone to reaction, the reaction is more intense and the reaction process is more rapid.

**3.2.3 Reactions.** Table 2 shows the main reactions of cocrystal structure and amorphous structure system in the first 10 ps under the shock wave with different velocities. It can be observed that the polymerizations of reactants occur in the system under various conditions. From the frequencies of reactions, the polymerizations between CL-20 and TNT

molecules are more likely to occur. Comparing the main responses of amorphous structural under shock waves with different velocities, it can be found that at 6 km s$^{-1}$, the overall reaction degree of the system is low, and the reaction frequencies of various reactions are relatively low. Under the shock waves with velocities of 7–9 km s$^{-1}$, the frequencies of polymerization reactions are relatively close, and the frequencies of decomposition reactions increase significantly with the increase of shock wave strength. Especially when the shock wave reaches 9 km s$^{-1}$, there is a mutual conversion of N-containing intermediates and N$_2$ in the high-frequency reactions, indicating that he reaction reaches a high degree. For cocrystal structure, with the increase of shock wave velocity, the

**Table 2** The initial reactions in shocked amorphous structure and cocrystal structure within 10 ps

| | Systems | | | |
| --- | --- | --- | --- | --- |
| | Disorder | | Co-crystal | |
| Velocities (km s$^{-1}$) | Total reaction number | High frequency reaction (the numbers in parentheses are the frequencies of occurrence) | Total reaction number | High frequency reaction (the numbers in parentheses are the frequencies of occurrence) |
| 6 | 13 | $(5)C_6H_6O_{12}N_{12} + C_7H_5O_6N_3 \rightarrow C_{13}H_{11}O_{18}N_{15}$<br>$(1)C_6H_6O_{12}N_{12} + C_6H_6O_{12}N_{12} \rightarrow C_{12}H_{12}O_{24}N_{24}$<br>$(1)C_{13}H_{11}O_{18}N_{15} \rightarrow C_{13}H_{11}O_{16}N_{14} + NO_2$<br>$(1)C_{13}H_{11}O_{16}N_{14} + NO_2 \rightarrow C_6H_6O_{12}N_{12} + C_7H_5O_6N_3$<br>$(1)C_6H_6O_{12}N_{12} \rightarrow C_6H_6O_{10}N_{11} + NO_2$ | N/A | |
| 7 | 125 | $(16)C_6H_6O_{12}N_{12} + C_7H_5O_6N_3 \rightarrow C_{13}H_{11}O_{18}N_{15}$<br>$(8)C_6H_6O_{12}N_{12} + C_6H_6O_{12}N_{12} \rightarrow C_{12}H_{12}O_{24}N_{24}$<br>$(5)C_{13}H_{11}O_{18}N_{15} \rightarrow C_6H_6O_{11}N_{12} + C_7H_5O_7N_3$<br>$(4)C_6H_6O_{12}N_{12} \rightarrow C_6H_6O_{10}N_{11} + NO_2$<br>$(3)C_{13}H_{11}O_{18}N_{15} + C_6H_6O_{12}N_{12} \rightarrow C_{19}H_{17}O_{30}N_{27}$ | 19 | $(3)C_6H_6O_{12}N_{12} + C_7H_5O_6N_3 \rightarrow C_{13}H_{11}O_{18}N_{15}$<br>$(2)C_6H_6O_{12}N_{12} + C_6H_6O_{12}N_{12} \rightarrow C_{12}H_{12}O_{24}N_{24}$<br>$(2)C_{12}H_{12}O_{24}N_{24} \rightarrow C_6H_6O_{11}N_{12} + C_6H_6O_{13}N_{12}$<br>$(2)C_{12}H_{12}O_{24}N_{24} + C_7H_5O_6N_3 \rightarrow C_{19}H_{17}O_{30}N_{27}$<br>$(1)C_6H_6O_{12}N_{12} + C_6H_6O_{12}N_{12} + C_6H_6O_{12}N_{12} \rightarrow C_{18}H_{18}O_{36}N_{36}$ |
| 8 | 2424 | $(14)C_6H_6O_{12}N_{12} + C_7H_5O_6N_3 \rightarrow C_{13}H_{11}O_{18}N_{15}$<br>$(10)C_6H_6O_{12}N_{12} \rightarrow C_6H_6O_{10}N_{11} + NO_2$<br>$(10)C_{13}H_{11}O_{18}N_{15} + C_7H_5O_6N_3 \rightarrow C_{20}H_{16}O_{24}N_{18}$<br>$(10)C_6H_6O_{12}N_{12} + NO_2 \rightarrow C_6H_6O_{14}N_{13}$<br>$(7)C_6H_6O_{12}N_{12} + C_6H_6O_{12}N_{12} \rightarrow C_{12}H_{12}O_{24}N_{24}$ | 699 | $(8)C_6H_6O_{12}N_{12} + C_7H_5O_6N_3 \rightarrow C_{13}H_{11}O_{18}N_{15}$<br>$(8)C_6H_6O_{12}N_{12} + C_6H_6O_{12}N_{12} \rightarrow C_{12}H_{12}O_{24}N_{24}$<br>$(7)C_6H_6O_{12}N_{12} \rightarrow C_6H_6O_{10}N_{11} + NO_2$<br>$(6)C_{13}H_{11}O_{18}N_{15} + C_7H_5O_6N_3 \rightarrow C_{20}H_{16}O_{24}N_{18}$<br>$(5)C_7H_5O_6N_3 + C_7H_5O_6N_3 \rightarrow C_{14}H_{10}O_{12}N_6$ |
| 9 | 3200 | $(15)C_6H_6O_{12}N_{12} + C_7H_5O_6N_3 \rightarrow C_{13}H_{11}O_{18}N_{15}$<br>$(14)C_6H_6O_{12}N_{12} \rightarrow C_6H_6O_{10}N_{11} + NO_2$<br>$(10)N_3O_3 \rightarrow NO_3 + N_2$<br><br>$(6)C_6H_6O_{12}N_{12} + C_6H_6O_{12}N_{12} \rightarrow C_{12}H_{12}O_{24}N_{24}$<br>$(5)NO_2 + NO_3 \rightarrow N_2O_5$ | 3490 | $(21)C_6H_6O_{12}N_{12} + C_7H_5O_6N_3 \rightarrow C_{13}H_{11}O_{18}N_{15}$<br>$(8)C_6H_6O_{12}N_{12} + C_6H_6O_{12}N_{12} \rightarrow C_{12}H_{12}O_{24}N_{24}$<br>$(6)C_6H_6O_{12}N_{12} \rightarrow C_6H_6O_{10}N_{11} + NO_2$<br>$(6)C_7H_5O_6N_3 + NO_2 \rightarrow C_7H_5O_8N_4$<br>$(6)C_{26}H_{22}O_{34}N_{29} \rightarrow C_{26}H_{22}O_{32}N_{28} + NO_2$ |

frequencies of polymerization reactions increase gradually, and some decomposition reactions appear. Comparing the amorphous structure and the cocrystal structure under the shock waves with the same velocity, the total reaction numbers of amorphous structure are more (except 9 km s$^{-1}$). In the high-frequency reactions, the decomposition reactions of amorphous structure account for a higher proportion, while the polymerization reactions of cocrystal structure account for a higher proportion. Especially when the shock wave velocity reaches 9 km s$^{-1}$, the total reaction number of amorphous structure is slightly lower than that of cocrystal structure. But there is a mutual conversion of small molecules containing N in the high-frequency reaction of amorphous structure, and the proportion of polymerization reactions in cocrystal structure is still very high.

## 3.3 Cluster

### 3.3.1 Number of clusters.
In this paper, the products with molecular weight greater than a CL-20 molecular are defined clusters. Fig. 7 is the evolution curve of the number of clusters in the amorphous structure and cocrystal structure system under the shock wave with velocities of 7–9 km s$^{-1}$. At 7 km s$^{-1}$, the number of clusters in the system is increasing within 50 ps. The number of clusters in the amorphous structure system is significantly more than that in the cocyrstal structure. Under the action of this shock wave, the movement rate of atoms in the system increases, the probability of mutual collision increases, and carbon containing clusters continue to be produced. Due to the low degree of decomposition reaction, clusters gradually accumulate, resulting in the gradual increase of their number.

Compared with cocrystal structure, amorphous structure is easier to be compressed, and the atomic collision probability in the system is higher, resulting in more clusters in the system. At 8 km s$^{-1}$, the number of clusters in the system first increases rapidly and then decreases gradually. Under the action of this stronger shock wave, the atom velocity in the system is faster, the collisions are more frequent, and the carbon containing clusters can accumulate to a certain number more quickly in the initial stage. Subsequently, due to the decomposition reaction,

the clusters are gradually decomposed into small molecules, and their number gradually decreases. In the initial stage, the clusters in the amorphous structure accumulate more rapidly. Then, due to the higher system temperature and the higher frequency of decomposition reaction, the number of clusters decreases rapidly, which is less than that in the cocrystal structure. At 9 km s$^{-1}$, the cluster number in the system increases in a very short time, reaches the peak value and then decreases rapidly, and finally stabilizes. The difference between the two systems is small. It takes less time for amorphous structures to move to the next stage.

### 3.3.2 Mass ratio of clusters.
There are great differences in the size of clusters, so the evolution of the number of clusters can not fully reflect the overall situation. It is also necessary to analyze the mass proportion of clusters in the system. Fig. 8 shows the change curve of cluster mass ratio in the two systems under the shock wave with velocities of 7–9 km s$^{-1}$. At 7 km s$^{-1}$, the mass ratio of clusters in the two systems is increasing, and there is a great difference. At 50 ps, the mass ratio of clusters in amorphous structure is 0.68, while that in cocrystal structure is only 0.23. At 8 km s$^{-1}$, the mass ratio of clusters increases gradually at first, reaches the peak value and then decreases. The overall change trend of the mass ratio is similar to that of the number. The mass ratio of amorphous clusters is 0.54 at 50 ps, and the cocrystal structure is 0.79. A large number of carbon atoms in the cocrystal structure are bound in the clusters, which makes it difficult for the system to generate $CO_2$. At 9 km s$^{-1}$, the mass ratio of clusters first increases rapidly and then decreases continuously, which is different from the number of clusters. After 20 ps, although the number of clusters increased slowly, the mass ratio continued to decline, indicating that the size of clusters gradually decreased under the action of decomposition reaction. In addition, after 20 ps, the number of clusters in the two systems is close, but the mass ratio of amorphous structure is significantly less than that of cocrystal structure, that is, the clusters in amorphous structure tend to exist in the form of small size.

Experiments show that energetic materials will produce a large amount of carbon black in the process of detonation.
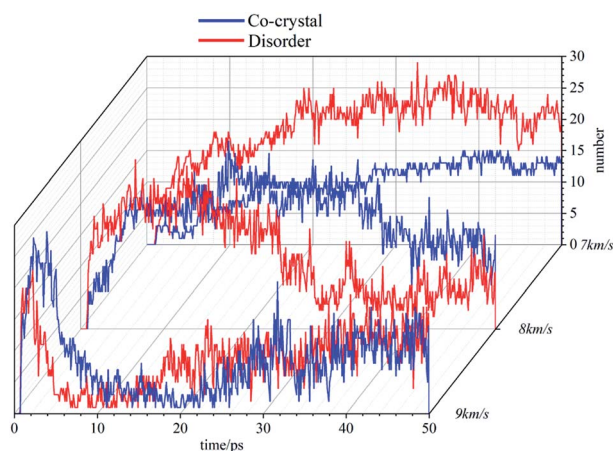


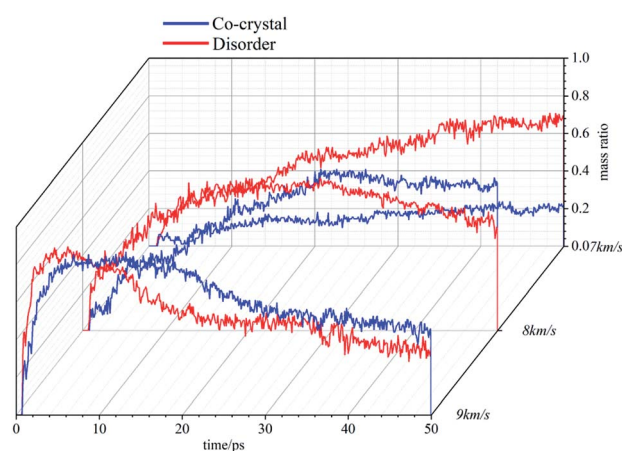Fig. 7 Evolution of cluster number.



Fig. 8 Mass ratio of clusters.

These carbon black are C-containing clusters, and their existence will seriously affect the decomposition of energetic materials. Through the previous analysis, it can be found that when the shock wave intensity is low (7 km s$^{-1}$), the amorphous structure is easier to be compressed, the atomic collision probability is higher, and more clusters are produced. With the shock wave intensity increases, the cluster size in the amorphous structure is smaller and more conducive to decomposition than that in the cocrystal structure. Many carbon atoms are bound in large-size clusters, which is difficult to decompose. The differences in clusters also affect the reaction process of the two systems, resulting in differences in the types and quantities of main products.

# 4 Conclusions

The CL-20/TNT cocrystal model and amorphous structure model are constructed respectively. The shock waves with velocities of 6–9 km s$^{-1}$ are applied to the two models by multiscale shock technology. The response processes of the two models under different shock waves are simulated. The thermodynamic evolution, reactants decay, products formation, main initial reactions and clusters evolution in the response process of the two models are compared and analyzed. The following conclusions are obtained:

(1) under the action of shock wave with the same velocity, the amorphous structure is easier to be compressed than the cocrystal structure, resulting in higher stress and higher temperature, and the corresponding chemical reaction is more intense. There is a strong linkage between the changes of various parameters.

(2) Because the chemical reaction in the amorphous structure is more intense, the reactants decay faster, the products are more abundant, and the intermediate products can complete the transformation to stable products earlier. NO$_2$ is the most important intermediate product, and its quantitative change can directly reflect the reaction process.

(3) Molecular polymers appear in the initial products. The polymerization between CL-20 and TNT is more likely to occur. In the first 10 ps, the amorphous structure is more prone to decomposition reaction, and the cocrystal structure is more prone to polymerization reaction.

(4) Under the shock wave with a velocity of 7 km s$^{-1}$, amorphous structure produces more clusters because it is easier to be compressed. When the shock wave velocity further increases, the cluster size in the amorphous structure is smaller and more conducive to decomposition.

# Conflicts of interest

There are no conflicts to declare.

# Acknowledgements

# Notes and references

1 C. Zhang, Y. Xiong, F. Jiao, M. Wang and H. Li, *Cryst. Growth Des.*, 2019, **19**, 1471–1478.
2 D. I. A. Millar, H. E. Maynard-Casely, D. R. Allan, A. S. Cumming, A. R. Lennie, A. J. Mackay, I. D. H. Oswald, C. C. Tang and C. R. Pulham, *CrystEngComm*, 2012, **14**, 3742–3749.
3 O. Bolton and A. J. Matzger, *Angew. Chem., Int. Ed.*, 2011, **50**, 8960–8963.
4 O. Bolton, L. R. Simke, P. F. Pagoria and A. J. Matzger, *Cryst. Growth Des.*, 2012, **12**, 4311–4314.
5 Z. Yang, H. Li, X. Zhou, C. Zhang, H. Huang, J. Li and F. Nie, *Cryst. Growth Des.*, 2012, **12**, 5155–5158.
6 Y. Wang, Z. Yang, H. Li, X. Zhou, Q. Zhang, J. Wang and Y. Liu, *Propellants, Explos., Pyrotech.*, 2014, **39**, 590–596.
7 H. Xu, X. Duan, H. Li and C. Pei, *RSC Adv.*, 2015, **5**, 95764–95770.
8 S. R. Anderson, P. Dubé, M. Krawiec, J. S. Salan, D. J. a. Ende and P. Samuels, *Propellants, Explos., Pyrotech.*, 2016, **41**, 783–788.
9 V. P. Sinditskii, A. N. Chernyi, S. Y. Yurova, A. A. Vasileva, D. V. Dashko and A. A. Astrat'ev, *RSC Adv.*, 2016, **6**, 81386–81393.
10 Q. Ma, T. Jiang, Y. Chi, Y. Chen, J. Wang, J. Huang and F. Nie, *New J. Chem.*, 2017, **41**, 4165–4172.
11 M. Ghosh, A. K. Sikder, S. Banerjee, M. B. Talawar and N. Sikder, *Def. Technol.*, 2020, **16**, 188–200.
12 C. Huang, J. Xu, X. Tian, J. Liu, L. Pan, Z. Yang and F. Nie, *Cryst. Growth Des.*, 2018, **18**, 2121–2128.
13 N. Liu, B. Duan, X. Lu, H. Mo, M. Xu, Q. Zhang and B. Wang, *CrystEngComm*, 2018, **20**, 2060–2067.
14 J. H. Urbelis, V. G. Young and J. A. Swift, *CrystEngComm*, 2015, **17**, 1564–1568.
15 Z. Yang, Q. Zeng, X. Zhou, Q. Zhang, F. Nie, H. Huang and H. Li, *RSC Adv.*, 2014, **4**, 65121–65126.
16 J. Zhang and J. n. M. Shreeve, *CrystEngComm*, 2016, **18**, 6124–6133.
17 C. Zhang, Y. Cao, H. Li, Y. Zhou, J. Zhou, T. Gao, H. Zhang, Z. Yang and G. Jiang, *CrystEngComm*, 2013, **15**, 4003–4014.
18 C. Zhang, X. Xue, Y. Cao, J. Zhou, A. Zhang, H. Li, Y. Zhou, R. Xu and T. Gao, *CrystEngComm*, 2014, **16**, 5905–5916.
19 R. Bu, Y. Xiong, X. Wei, H. Li and C. Zhang, *Cryst. Growth Des.*, 2019, **19**, 5981–5997.
20 R. Bu, Y. Xiong and C. Zhang, *Cryst. Growth Des.*, 2020, **20**, 2824–2841.
21 G. Liu, H. Li, R. Gou and C. Zhang, *Cryst. Growth Des.*, 2018, **18**, 7065–7078.
22 G. Liu, S.-H. Wei and C. Zhang, *Cryst. Growth Des.*, 2020, **20**, 7065–7079.
23 Q. Zeng, Y. Ma, J. Li and C. Zhang, *CrystEngComm*, 2017, **19**, 2687–2694.
24 D. Guo, Q. An, S. V. Zybin, W. A. Goddard III, F. Huang and B. Tang, *J. Mater. Chem. A*, 2015, **3**, 5409–5419.
25 X. Xue, Y. Ma, Q. Zeng and C. Zhang, *J. Phys. Chem. C*, 2017, **121**, 4899–4908.

26 C. Ren, X. Li and L. Guo, *J. Chem. Inf. Model.*, 2019, **59**, 2079–2092.

27 C. Ren, H. Liu, X. Li and L. Guo, *Phys. Chem. Chem. Phys.*, 2020, **22**, 2827–2840.

28 H. Liu, Y. Li, Z. Ma, Z. Zhou, J. Li and Y. He, *Acta Phys.-Chim. Sin.*, 2019, **35**, 858–867.

29 X.-Q. Zhang, X.-R. Chen, S. Kaliamurthi, G. Selvaraj, G.-F. Ji and D.-Q. Wei, *J. Phys. Chem. C*, 2018, **122**, 24270–24278.

30 Y. Li, W.-L. Yu, H. Huang, M. Zhu and J.-T. Wang, *RSC Adv.*, 2021, **11**, 38383–38390.

31 V. P. Sinditskii, N. V. Yudin, S. I. Fedorchenko, V. Y. Egorshev, N. A. Kostin, L. V. Gezalyan and J.-G. Zhang, *Thermochim. Acta*, 2020, **691**, 178703.

32 M. Sakano, B. Hamilton, M. M. Islam and A. Strachan, *J. Phys. Chem. C*, 2018, **122**, 27032–27043.

33 G. D. Smith and R. K. Bharadwaj, *J. Phys. Chem. B*, 1999, **103**, 3570–3575.

34 E. J. Reed, L. E. Fried and J. D. Joannopoulos, *Phys. Rev. Lett.*, 2003, **90**, 235503.

35 L. Liu, Y. Liu, S. V. Zybin, H. Sun and W. A. Goddard, *J. Phys. Chem. A*, 2011, **115**, 11016–11022.